International Journal of Heat and Mass Transfer 158 (2020) 120034

Contents lists available at ScienceDirect

International Journal of Heat and Mass Transfer

journal homepage: www.elsevier.com/locate/hmt

Numerical study on the heat transfer and pressure drop characteristics of fin-and-tube surface with four round-convex strips around each tube

Xiao-Yu Li[a], Yu-Tong Mu[b], Zhao-Hui Li[a], Wen-Quan Tao[a,*]

[a] Key Laboratory of Thermo-Fluid Science and Engineering of MOE, Xi'an Jiaotong University, Xi'an, Shaanxi 710049, China
[b] School of Human Settlements and Civil Engineering, Xi'an Jiaotong University, Xi'an, Shaanxi 710049, China

ARTICLE INFO

Article history:
Received 4 February 2020
Revised 19 May 2020
Accepted 30 May 2020
Available online 30 June 2020

ABSTRACT

In this paper, a three-dimensional numerical investigation is performed for both heat transfer and pressure drop of a new kind of slit fin applied to heat exchangers in air compression industry by FLUENT. A comparison between this new slit fin and normal plain fin is made. It is found that the flow and heat transfer come into full development stage after 12 rows. The effects of seven different parameters on the fully developed heat transfer performance are examined and all the calculation results agree well with the field synergy principle.Among these parameters,reducing spanwise fin pitch has the largest performance improvement. The optimum values are found for the height of slit and the length of rear slit. The correlations for j and f factors are proposed, which take four and five dimensionless geometric parameters into consideration, respectively.

1. Introduction

Fin-and-tube heat exchangers are widely used in industries and daily life. In most fin-and-tube heat exchangers, heat transfer occurs between air and some liquid (water or refrigerants). In order to improve the efficiency of the heat exchangers, it is essential to enhance airside heat transfer which usually accounts for more than 90 percent of the overall thermal resistance [1]. Since the first paper on enhanced heat transfer published by Joule[2] about 150 years ago, a large number of researches on enhancing heat transfer have been conducted. Especially after 1950, a lot of new types of fin surface have been developed to enhance airside heat transfer. In all of these enhanced heat transfer surfaces, slotted fin surface (including louvered fin and strip fin) is the one widely employed because of its high heat transfer coefficient and acceptable pressure drop penalty, and a large amount of investigations have been conducted on it.

To the authors' knowledge, the first research on slotted fin surface was conducted by Nakayama and Xu [3] in 1983. Their investigation found that at 3 m/s air velocity the heat transfer coefficient of the slotted fin surface is 78% higher than that of the plain fin surface. Yun and Lee [4] analyzed their experimental data of plain fin, louvered fin and three types of slotted fins by scaled-up models. Their results showed that the louvered fin surface has the highest heat transfer rate and highest pressure drop which is too high to prevent its extensive application and they recommended the slotted fin surfaces with strips paralleled to the plain fin surface for engineering application. Wang et al. [5-6] and Du et al. [7] made a series of experimental study on heat transfer and pressure drop of slit and louver fin surface. In paper [5] 49 samples with different fin pitch, louver pitch, louver height, longitudinal tube pitch, transverse tube pitch and tube diameter were studied and the correlations for j and f factors based on the experimental data were proposed. The heat transfer and friction correlations for slit fin-and-tube heat exchangers were also proposed in references [6] and [7]. The final correlation in [7] takes the effect of Reynolds number, fin pitch, number of slits, number of longitudinal tube rows, longitudinal tube pitch, transverse tube pitch, tube diameter, height of slit and width of slit into consideration which can be much more widely used than the first correlation proposed in [3]. Balatka et al.[8] made experimental studies on five tube-and-fin heat exchangers (four with slits) and investigated the relationship between heat transfer and flow behavior by means of dye injection and hydrogen bubble visualization techniques. Their results recommended that the slots should be arranged around the tubes to reduce the size of wake area behind the tubes. In recent years, investigation on slit fin-and-tube heat exchanger on wet condition is a hotspot in the study of enhanced heat transfer. Since this subject is outside the major concern of the present paper, no further

* Corresponding author.
E-mail address: wqtao@mail.xjtu.edu.cn (W.-Q. Tao).

https://doi.org/10.1016/j.ijheatmasstransfer.2020.120034
0017-9310/

Nomenclatures

A	area(m^2)
A_c	minimum flow area (m^2)
A_o	total surface area (m^2)
c_p	specific heat ($Jkg^{-1}K^{-1}$)
D	tube outside diameter(m)
f	friction factor
F_p	fin pitch(m)
h	heat transfer coefficient ($Wm^{-2}K^{-1}$)
H_c	height of the convex(m)
j	Colburn factor
k	turbulent kinetic energy(m^2s^{-2})
L_p	longitudinal fin pitch(m)
N	number of tube rows
Nu	Nusselt number
p	pressure (Pa)
P	pumping power(W)
Pr	Prandtl number
Q	mass flow rate(kgs^{-1})
Re	Reynolds number
S_1	length of the frontal strip(m)
S_2	length of the rear strip(m)
S_p	spanwise fin pitch(m)
T	temperature(K)
u	velocity(ms^{-1})

Greek symbols

Δp	pressure drop (Pa)
Δt	temperature difference(K)
ΔT	Log mean temperature difference(K)
ρ	density(kgm^{-3})
μ	viscosity($kgm^{-1}s^{-1}$)
λ	thermal conductivity ($Wm^{-1}K^{-1}$)
ε	turbulent energy dissipation rate(m^2s^{-3})
Φ	heat transfer rate(W)
β	local intersection angle (Deg.)

Subscripts

in	inlet
out	outlet
max	maximum
m	mean
w	tube wall

review will be presented and the interested readers may consult [9-12].

All the researches mentioned above are experimental investigation. Numerical study is another important method in the investigation of enhanced heat transfer. Compared with experimental investigation, the cost of numerical research is much lower and the scope of research can be extended outside the test conditions. Qu et al.[13] made a numerical computation for two-row strip fin surface with X-arrangement of strips. Results show that the strip fin with strips located in the downstream part of the fin surface has higher heat transfer rate and they explained this result by field synergy principle [14,15]. Cheng et al. [16] also performed a numerical investigation on three types of slit fin surfaces and a plain fin surface. With the same number of strips, the slit fin with the strips positioned front sparse and rear dense has the best heat transfer performance. The best slit fin can increase the heat transfer coefficient by 86% compared with plain fin. Zhou and Tao [17] found that the slotted fin performed better under the identical pumping power constraint if the strips mainly located in the rear part. Jin et al. [18] studied 15 slotted fin surfaces, and found that their j/f versus Re curves cross with the curve of the plain plate fin surface at some turning Reynolds number, beyond which the j/f ratio of slotted fin surfaces is higher than that of plain plate fin surfaces, and vice versa. Tao et al. [19] studied the effect of strip arrangement in detail. They draw a conclusion that the slit fin has the best heat transfer performance when the front and rear part have the same thermal resistance. Wu and Tao [20,21] investigated the influence of some main parameters of longitudinal vortex generator (LVG) including the location of LVG in the channel, geometric size and shape of LVG on heat transfer enhancement by numerical method, and found that it was the improvement in the synergy between velocity and temperature gradient that was the basic mechanism of LVG enhancing heat transfer. Li et al.[22] performed a 3-D numerical simulation on a slit fin-and-tube heat exchanger with longitudinal vortex generators. The comparison among this new novel heat transfer surface, heat transfer surface with X-shape arrangement of slit fin and heat transfer surface with longitudinal vortex generators showed that the novel heat transfer surface had medium values of j and f factors and the highest value of $j/f^{1/3}$ factor. Fan et al.[23] made a numerical research in order to find out a new structure to replace a three-row wavy fin-and-tube surface by a two-row fin-and-tube surface with this new structure. Finally, a new structure with a combination of LVGs and strips was proposed which can satisfy the requirement. Wu et al.[24] proposed a new semi-dimpled slit fin and investigated the effects of several parameters including fin pitch, arrangement of semi-dimple and dimple radius on the performance of the new fin surface. The computation result showed that when $Re>1521$ the overall performance of the semi-dimpled slit fin was better than that of slit fin. Wu et al. [25] made another numerical investigation on a composite fin with both strips and longitudinal vortex generators. This new composite fin has better heat transfer performance compared with slit fin. Li et al.[26] proposed a new kind of plain fin with winglets arranged around each tube and compared its heat transfer and pressure drop performance with a wavy fin surface, a common-flow-down LVGs fin surface and a plain fin surface. The result showed that this new LVGs surface had the best performance. Sarpotdar et al.[27] proposed correlations for slit fins with tube diameters less than 5 mm by numerical study. Another composite fin consisted of louver and slit was numerically investigated by Park et al.[28]. The $j/f^{1/3}$ factor of the optimized composite fin they designed was 6.1% higher than that of the X-shaped slit fin. By conjugated simulation Mutlu and Kilic [29] investigated how the fin material thermal conductivity influencedthe effects of Reynolds number, tube diameter, fin pitch, fin thickness and fin length on Nusselt number. A new correlation that considered the effect of fin material thermal conductivity was proposed.

As cited above, in 1998, Guo et al. [14,15] proposed a novel concept which is now called the field synergy principle to reveal the mechanism of heat transfer enhancement. The principle indicates that reducing the intersection angle between velocity and temperature gradient is the basic mechanism for enhancing single phase convective heat transfer. Since then a lot of studies [30-34] made further verification and applications. Recently a comprehensive review of the FSP was conducted by He and Tao in [35], and interested readers are recommended to consult and detail introduction is omitted here for simplicity. The FSP will be adopted in the analysis of our numerical results.

Although great efforts have been made for enhancing airside heat transfer, and lots of enhancing techniques have been proposed and adopted, however, among the existing enhanced techniques there are some shortages from mechanical and manufacturing points of view. The enhancing structures are usually slotted fin and/or longitudinal vortex generators, with which the fin material strength may be somewhat deteriorated. In addition, the mouths of the slots are usually normal to the oncoming flow which may in-

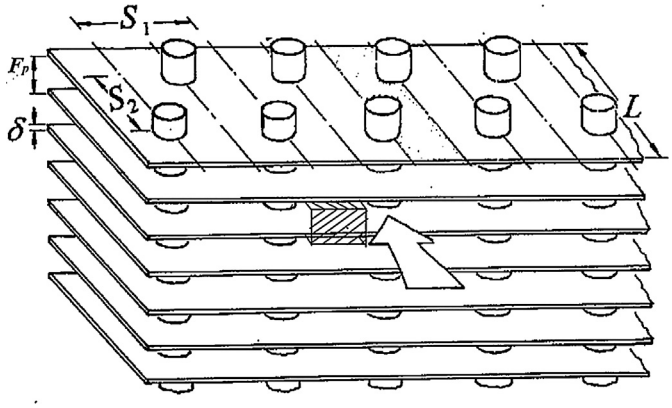

Fig. 1. Schematic diagram of a two rows plain fin-and-tube heat transfer exchanger.

Table 1
Geometry parameters of the finned tube in physical model.

Parameter	Value
Fin pitch F_p(mm)	2.3
Fin thickness δ(mm)	0.15
Tube diameter D_c (mm)	18
Transverse tube spacing Sp (mm)	42
Longitudinal tube spacing Lp (mm)	36.373
Tube row No. N	2–14

crease the pressure drop significantly while enhancing heat transfer. In this paper, based on practice of air cooler made in some Chinese factory, numerical study of heat transfer will be conducted between dry air and a protruded strip fin with strips around tubes, named round-convex fin. The effects of a number of parameters such as Reynolds number, number of tube rows, height of strips, etc. are examined, and the results are compared with the plain plate-fin-and tube surface.

In the following presentation, the description of geometric model and numerical method are presented in Section 2. Data reduction and some preliminary computations are presented in Section 3. Then computation results are discussed in Section 4, and finally some conclusions are drawn in Section 5.

2. Model description and numerical method

A schematic diagram of a two-row plain fin-and-tube heat transfer exchanger is shown in Fig. 1, and the plain fin-and-tube surface will be served as the reference for comparison. The geometric parameters of the basic plate fin are listed in Table 1. The round-convex fin studied in this paper is machined based on the plain fin. A picture of the round-convex fin is shown in Fig. 2(a), and its geometries are presented in Fig. 2(b) and (c). The tubes are made of copper and the fins are made of aluminum.

Because of the periodicity of the structure in both spanwise (y-axis) and vertical (z-axis) directions, we can take one unit as the computational domain, schematically shown by the shaded area in Fig. 1. For the case studied, the upper interface of the computational domain is 1.65 mm above the basic fin surface and the lower interface is 0.5 mm below the basic fin surface, which is shown by the dashed lines in Fig. 2(c). The 3D full computation domain is schematically shown in Fig. 3, where streamwise tube row number can be varied from 2 to 14 in the simulation.

The fluid is assumed to be incompressible and the properties are assumed to be constant. Two different series of properties are tested to confirm that the constant property assumption is applicable. The fluid properties and the simulation results are shown in

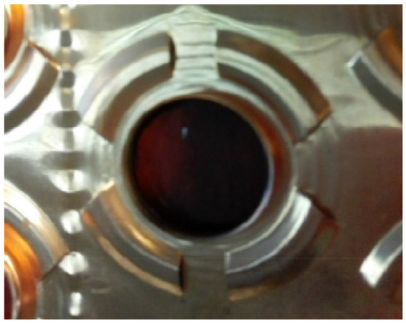

(a) Picture of round-convex fin

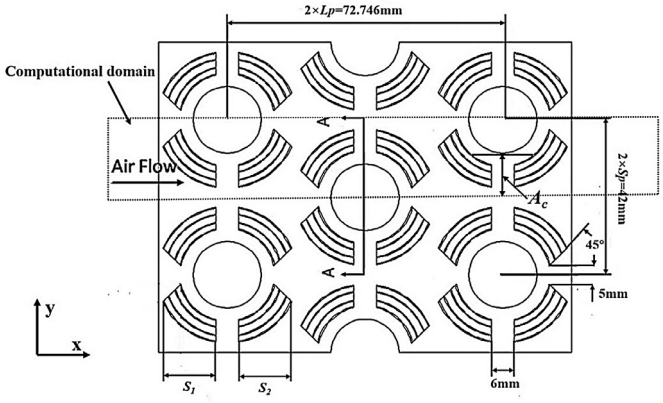

(b) Top view

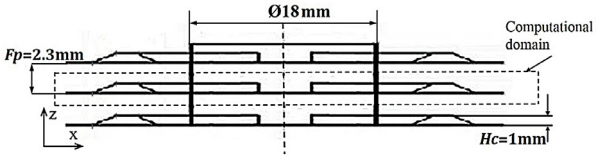

(c) Side view

Fig. 2. Picture and geometry of round-convex fin surface.

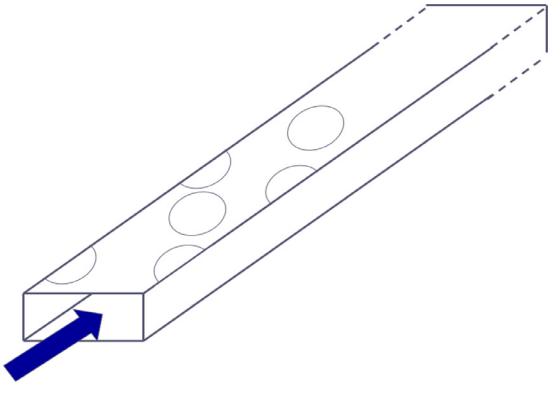

Fig. 3. Computational domain (not in scale).

Table 2. It can be seen that at the same Reynolds number, the variation in Nusselt number is about 3% and the two friction factors are almost the same. Since the fluid properties were determined by the reference temperature (taking the averaged value of inlet and outlet), so the constant properties assumption is still suitable for the simulation. The flow is turbulent. Both the fluid flow and the heat transfer are in steady state condition. The tube temperature is assumed to be constant because the heat transfer coefficient

Table 2
Comparison of simulation result with different fluid property.

Parameter	Density (kg/m^3)	Thermal conductivity (W/m/K)	Viscosity (kg/m/s)	*Re*	*Nu*	*f*
Value	1.225	0.0242	1.7894×10^{-5}	6161	76.5	0.031
Value	0.746	0.0393	3.485×10^{-5}	6165	74.1	0.031

inside the tube is always much higher than the heat transfer coefficient outside the tubes and the material of tube has high thermal conductivity. The temperature of the fin surface is obtained by conjugated simulation in which the energy equations for both air and fin are solved simultaneously [36].

The governing equations for continuity, momentum and energy can be described as follows:

Continuity equation:

$$\frac{\partial}{\partial x_i}(\rho u_i) = 0 \tag{1}$$

Momentum equation:

$$\frac{\partial}{\partial x_i}(\rho u_i u_k) = \frac{\partial}{\partial x_i}\left(\mu \frac{\partial u_k}{\partial x_i}\right) - \frac{\partial p}{\partial x_k} \tag{2}$$

Energy equation:

$$\frac{\partial}{\partial x_i}(\rho u_i T) = \frac{\partial}{\partial x_i}\left(\Gamma \frac{\partial T}{\partial x_i}\right) \tag{3}$$

where $\Gamma = \lambda/c_p$.

The realizable k-ε turbulence model [37] is adopted in the simulation:

$$\rho\frac{\partial \varepsilon}{\partial t} + \rho u_j \frac{\partial \varepsilon}{\partial x_j} = \frac{\partial}{\partial x_j}\left[\left(\mu + \frac{\mu_t}{\sigma_\varepsilon}\right)\frac{\partial \varepsilon}{\partial x_j}\right] + C_1\rho(2S_{ij}{}^2)^{1/2}\varepsilon - C_2\rho\frac{\varepsilon^2}{k+\sqrt{\mu_t\varepsilon}} \tag{4}$$

$$\rho\frac{\partial k}{\partial t} + \rho u_j \frac{\partial k}{\partial x_j} = \frac{\partial}{\partial x_j}\left[\left(\mu + \frac{\mu_t}{\sigma_k}\right)\frac{\partial k}{\partial x_j}\right] + \mu_t S^2 - \rho\varepsilon \tag{5}$$

where $\mu_t = \rho C_\mu \frac{k^2}{\varepsilon}$ and the C_μ is given by:

$$C_\mu = \frac{1}{A_0 + A_s\frac{U^* k}{\varepsilon}} \tag{6}$$

where $A_0 = 4.04$, $A_s = \sqrt{6}\cos\varphi$, $\varphi = \frac{1}{3}\cos^{-1}[\sqrt{6}\frac{S_{ij}S_{jk}S_{ki}}{(\sqrt{S_{ij}S_{ij}})^3}]$ and S_{ij} is the parameter that shows the variation of velocities in different directions.

$$S_{ij} = \frac{1}{2}\left(\frac{\partial u_j}{\partial x_i} + \frac{\partial u_i}{\partial x_j}\right) \tag{7}$$

The other parameters of the model are C_2=1.9, σ_k=1.0, σ_ε=1.2. The detailed introduction of the turbulent model can be found in Ref. [37].

The boundary conditions are set up as follows. At the inlet boundary, the air entering the computational domain is assumed to have a constant velocity u_{in} in x direction and a constant temperature T_{in} (500 K), and the velocities in y and z directions are assumed to be zero. At the outlet boundary, outflow boundary condition is adopted ($\frac{\partial u}{\partial x} = \frac{\partial v}{\partial x} = \frac{\partial w}{\partial x} = \frac{\partial T}{\partial x} = 0$). Symmetric boundary with the derivatives normal to the boundary being assumed zero are adopted at the left and right boundaries. At the tube region, the temperature of tube wall T_w is assumed to be constant (300 K). Periodic boundary conditions are adopted at the top and bottom boundaries. At the solid surface, no-slipping condition for velocities is selected.

The above governing equations are solved by commercial software FLUENT with second-order discretization scheme for both convective and diffusive terms. The computation is regarded as converged when the residual for each variable is less than 1.0×10^{-4} and the variations of temperature and pressure at the middle position and outlet of fin are less than 0.01 K and 0.01 Pa in 1000 iterations, respectively.

3. Data reduction and preliminary computation

3.1. Parameter definition

The heat transfer rate and heat transfer coefficient are determined by the following equations:

$$\phi = A_f u_{in}\rho c_p(T_{in} - T_{out}) \tag{8}$$

$$h = \frac{\phi}{A_{total}\Delta T} \tag{9}$$

where A_f is the area of air inlet, u_{in} is the air velocity at the inlet, h is the averaged heat transfer coefficient and A_{total} is the total heat transfer area:

$$A_{total} = A_{tube} + A_{fin}\eta \tag{10}$$

A_{tube} is the area of tube and A_{fin} is the area of fin. η is fin efficiency:

$$\eta = \phi/\phi_{ideal} \tag{11}$$

ϕ_{ideal} is calculated by setting the temperature of fin equal to the temperature of tube wall and is determined during simulation.

$$\text{and} \qquad \Delta T = \frac{T_{in} - T_{out}}{\ln\frac{T_{in}-T_w}{T_{out}-T_w}} \tag{12}$$

T_{in} and T_{out} are the average temperatures at inlet and outlet. T_w is the temperature of tube wall.

Parameters used in the simulation are introduced as follows:

$$Nu = \frac{hD}{\lambda} \tag{13}$$

$$Re = \frac{\rho u_{\max} D}{\mu} \tag{14}$$

$$j = \frac{Nu}{RePr^{1/3}} \tag{15}$$

$$\Delta p = p_{in} - p_{out} \tag{16}$$

$$P = \Delta p u_{in} A_f = \Delta p u_{max} A_c \tag{17}$$

There are several different definitions of friction factor. In this paper we use the definition in Ref. [38]:

$$f = \frac{A_c}{A_o}\frac{\rho_m}{\rho_{in}}\left[\frac{2*\Delta p\rho_{in}}{(\rho_m u_{\max})^2} - (1+\sigma^2)\left(\frac{\rho_{in}}{\rho_{out}} - 1\right)\right] \tag{18}$$

Because properties are assumed to be constant in the simulation, Eq. (18) can be simplified to

$$f = \frac{A_c}{A_o} * \frac{2\Delta p}{\rho u_{\max}{}^2} \tag{19}$$

Among these equations, D is the outside diameter of tube wall, A_c is the minimum flow area shown in Fig. 2(b), $u_{\max}$ is the maximum velocity at the minimum flow area, p_{in} and p_{out} are the static

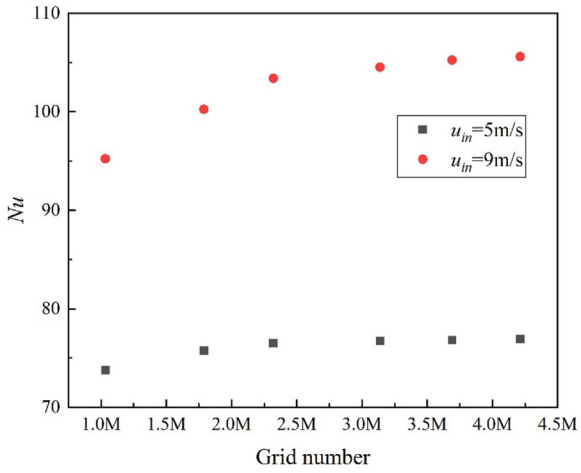

(a) Grid independent examination

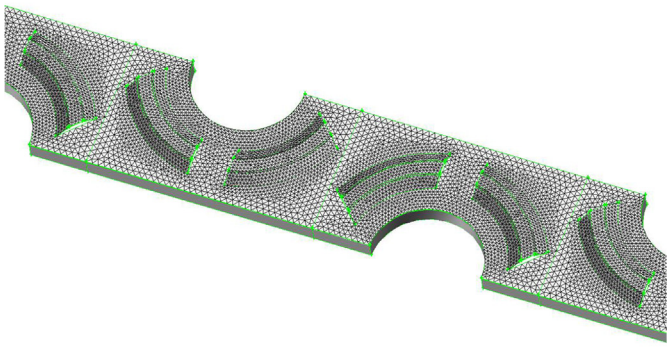

(b) Mesh schematic of fin surface

Fig. 4. Grid independent examination and mesh of four-row case.

pressure at inlet and outlet of fin surface, and A_o is the total surface area. It should be noted that the fluid properties were determined by a reference temperature which is the average of inlet and outlet temperatures.

In order to analyze the heat transfer by field synergy principle, the local intersection angle and volume weighted average intersection angle of the computational domain between the velocity and temperature gradient are defined respectively as follows:

$$\beta = \cos^{-1}\frac{u\frac{\partial T}{\partial x} + v\frac{\partial T}{\partial y} + w\frac{\partial T}{\partial z}}{\left|\vec{U}\right||\Delta T|} \tag{20}$$

$$\beta_m = \cos^{-1}\frac{\sum\left|\vec{U}\right|_i|\Delta T|_i\cos\beta_i dv_i}{\sum\left|\vec{U}\right|_i|\Delta T|_i dv_i} \tag{21}$$

where dv_i is the volume element of the control volume.

3.2. Grid independent examination

In order to conduct the grid independent examination, six different grid systems with grid number from 1.03 M to 4.21 M for four-row-tube model are investigated at two different frontal velocities equal to 5 m/s and 9 m/s. The predicted average *Nu* numbers of these grid systems are shown in Fig. 4(a). It can be seen that for both velocities the solution of 2.32 million grid system can be regarded as grid-independent-solution when take both calculation speed and calculation accuracy into consideration, and is adopted in the following computations for four-row-tube model. For all the numbers of tube rows studied (2–14) the corresponding number of cells are presented in Table 3. Fig. 4(b) presents the grid schematic diagram of the fin surface whose mesh density is one third of the practical one. It can be seen from the grid schematic diagram that the mesh is refined around tubes and convex plates.

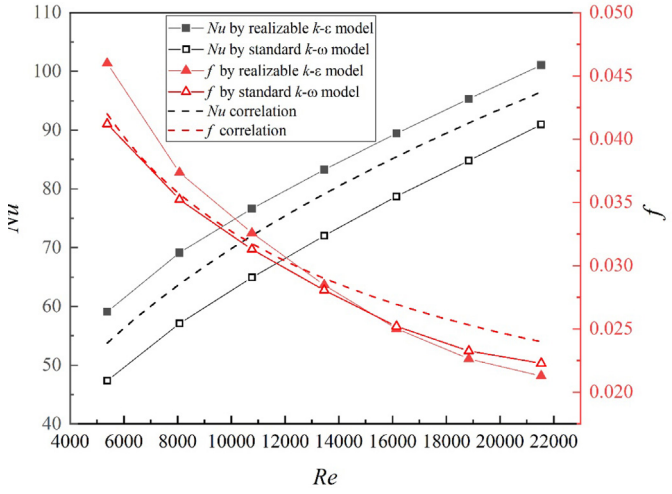

Fig. 5. Comparison of *Nu* and *f for* model validation.

3.3. Verification of the computational model

In order to verify the computational model, comparison is carried out between results of numerical and experimental investigation on the heat exchanger with round-convex-fin. The tested heat transfer surfaces have the same geometric parameters as shown in Table 4. The air velocity in the inlet ranges from 2 m/s to 8 m/s and the Reynolds number varies from 5383 to 21531.Two different turbulent models are applied in the simulation. The comparison between *Nu* and *f* predicted by the numerical model and the experimental correlations in paper [38] is shown in Fig. 5. For realizable k-ε model,the maximum deviation in the Nusselt number is 10% and averaged deviation is 6%. For standard k-ω model, the maximum deviation in Nusselt number is about 12% and averaged deviation is 10%. The realizabla k-ε model is finally applied in the simulation. The deviation of friction factor slope between test and numerical data is mainly comes from the following two aspects . Firstly, the experimental sample couldn't be so perfect as the numerical model, as can be witnessed from Figs. 2(a) and 4(b). There are some small bumpiness between adjacent round-convex fins in practical fin surface, but they do not exist in the numerical model, and the friction factor is sensitive to such geometrical structures. Secondly, the uncertainties of the experimental measurement and numerical turbulence model can also cause some deviation. Generally speaking, the agreement between test data and numerical results is satisfactory.

4. Results and discussion

In this section, we first compare the performance of plain fin and fin with four round-convex strips around each tube. Then the effects of number of tube rows, longitudinal tube pitch, spanwise tube pitch, fin pitch, height of strips and length of frontal and rear strips are analyzed respectively.

Table 3
Number of cells for different number of tube row.

Number of rows	2	4	6	8	10	12	14
Number of cells	1.29 million	2.32 million	3.35 million	4.38 million	5.41 million	6.44 million	7.47 million

Table 4
Geometry parameters of the finned tube in model validation.

Parameter	Value
Fin pitch F_p (mm)	2.3
Fin thickness δ (mm)	0.15
Tube diameter D_c (mm)	19.6
Transverse tube spacing S_p (mm)	42
Longitudinal tube spacing L_p (mm)	36.373
Tube row No. N	11

4.1. Comparison between round-convex fin and plain fin

The round-convex fin researched in this paper is enhanced based on the plain fin. So, discussion is started with the comparison between round-convex fin and plain fin. Both computation models have four rows of tubes and the inlet velocity vary from 3 m/s to 15 m/s. Fig. 6(a) presents the comparison of j factor between these two different fin surfaces. From Fig. 6(a) we can see that the j factor of convex fin is about 25 percent larger than that of plain fin. Fig. 6(b) presents the relations between friction factor f and Reynolds number of the two fins. From the figure we can see that the friction factor decreases with the increase of Re number and the f of convex is appreciably larger than that of plain fin at the same Re number. Within the range of Reynolds number studied, the friction factor of round-convex fin is averagely 33% larger than that of the plain fin. Within the Reynolds number range studied, the correlations between j and f factors with Re for the four-row surface are given as follows:

$$j = 1.74 \times Re^{-0.5823} \tag{22}$$

$$f = 9.31 \times Re^{-0.6103} \tag{23}$$

Comprehensive correlations for all the parameters studied will be presented in Section 4.3.

In practical application, attention is often paid to the overall performance like heat transfer under the same pumping power. Fig. 7 shows the relationship between two performance evaluation factors (PEFs) and Reynolds number. The black square point stands for the ratio of factor $j/f^{1/3}$ between round-convex fin and plain fin. This factor can represent the heat transfer rate under the identical pumping power constraint. The red circle point shows the ratio of $j/f^{1/2}$ which means the heat transfer rate under the same pressure drop constraint. It can be seen that all two PEFs are larger than 1 in the studied Reynolds number range which means that round-convex fin can enhance heat transfer under both identical pumping power and pressure drop conditions when Reynolds number varies from 5000 to 35000. In the following sections, factor $(j_c/f_c^{1/3})/(j_p/f_p^{1/3})$ is chosen to evaluate the overall performance. Since both heat transfer rate and pumping power are influenced by minimum flow area and length in air flow direction. So performance evaluation will only be performed for parameters of height and length of strips, since changes of these parameters will not affect the cross section area and the fin length in flow direction .

The temperature distributions in the section 0.5 mm above the fin surface of both the round-convex fin and plain fin when inlet velocity equals to 5 m/s are shown in Fig. 8. The velocity distribution of the same section is shown in Fig. 9. It can be seen that the round convexity fin can significantly reduce wake regions formed behind each tube because air is guided by the rear strip to flow around the tube.This can obviously enhance heat transfer. At the same time, air flowing over strips can also increase the disturbance and destroy the boundary layer. Air flows inside the strips also has better heat transfer performance. All of these reasons lead to a better heat transfer performance and a larger pressure drop. And the averaged outlet air temperature of the convex fin is lower than that of plain fin (Fig. 8).

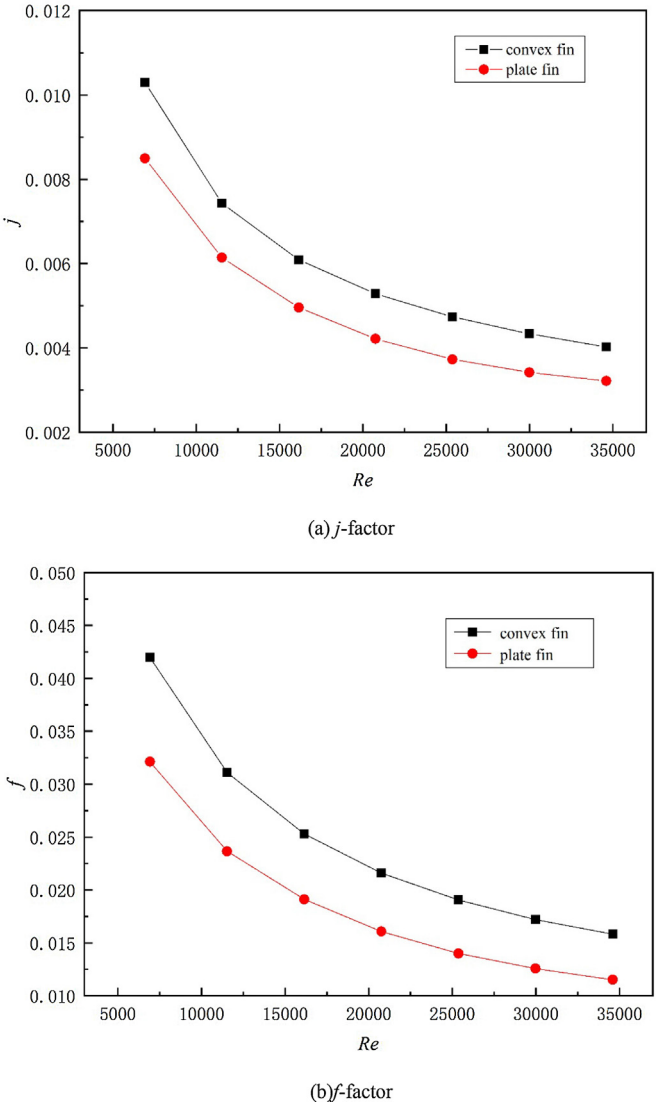

Fig. 6. j and f factors vs. Re for round-convex fin and plain fin of four-row.

4.2. Effects of six parameters

4.2.1. The effect of tube rows

In order to examine the effect of number of tube rows on the performance of round-convex fin, seven different number of tube rows from 2 to 14 was simulated. The other parameters remained the same as listed in Table 5. It is worth noting here that when study the effect of different parameters Reynolds number is re-

Table 5
Standard parameters of the fin.

Parameter	Value	Dimensionless value based on D_c
Fin pitch F_p (mm)	2.3	0.1278
Fin thickness δ (mm)	0.15	0.0083
Tube diameter D_c (mm)	18	1
Transverse tube spacing S_p (mm)	42	2.3333
Longitudinal tube spacing L_p (mm)	36.373	2.0207
Height of convex plate H_c (mm)	1	0.0556
Length of the frontal convexity S_1 (mm)	14	0.779
Length of the rear convexity S_2 (mm)	14	0.779
Tube row No. N	4	/

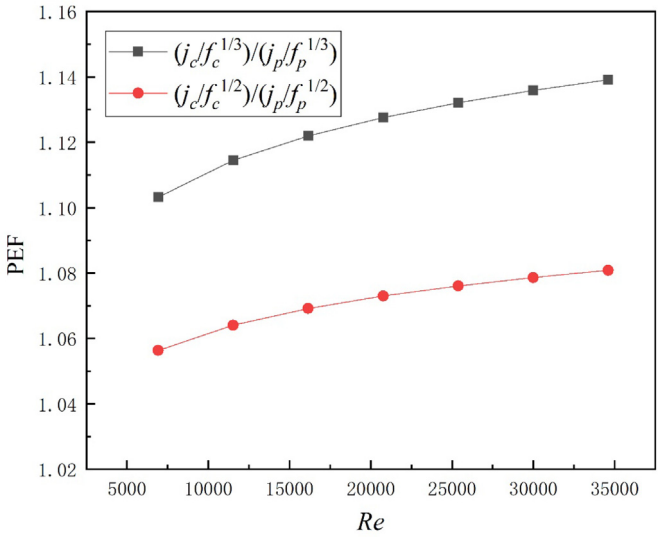

Fig. 7. Performance evaluation of round-convex fin.

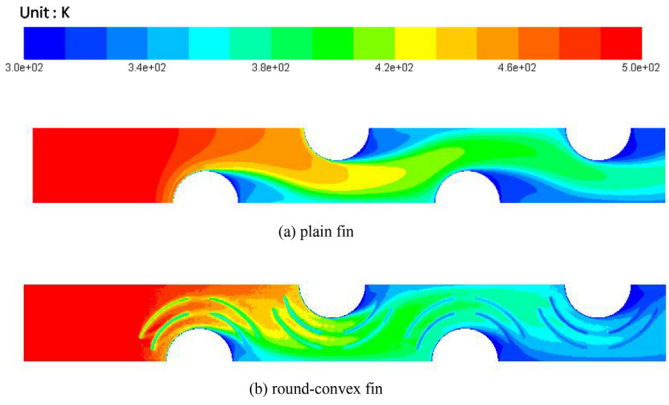

Fig. 8. Temperature distribution of plain fin and round-convex fin at section 0.5 mm above the fin surface.

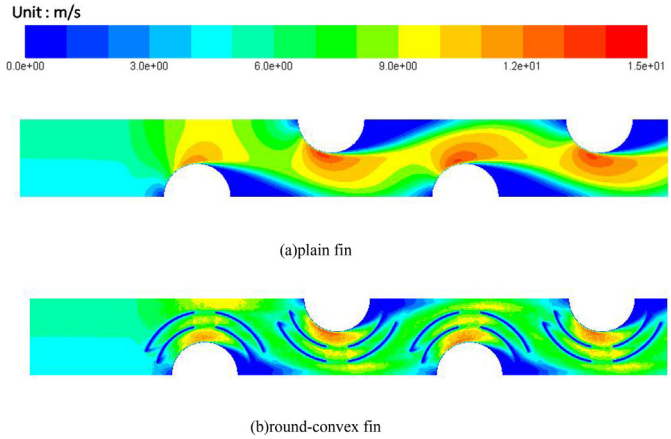

Fig. 9. Velocity distribution of plain fin and round-convex fin at section 0.5 mm above the fin surface.

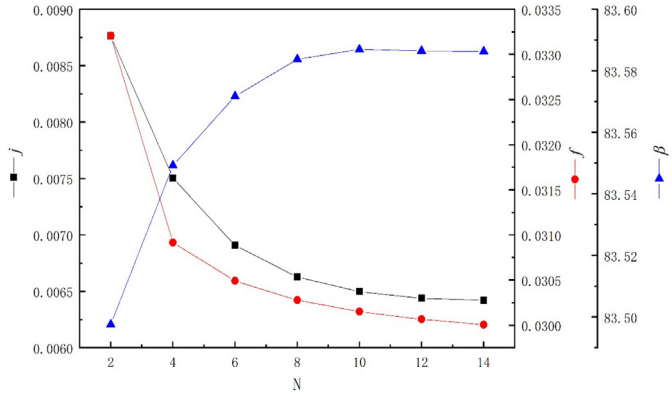

Fig. 10. The effect of tube row number on j factor, f factor and average intersectionangle.

mained at 11536 (u_{max}=9.36 m/s) and non-dimensional geometric parameters are based on the tube outside diameter.

Fig. 10 shows the effect of number of tube rows on the j factor, friction factorand synergy angle. From Fig. 10 we can see that the j factor and friction factor decrease with the increase of the number of tube rows but the changing trend becomes mild with the increase of row number. When the number of tube rows is larger than 12, the j factor and friction factor almost unchanged with further increase of number of tube rows. This implies that for the round-convex fin, air flow and heat transfer enter fully developed region after twelve rows. The average synergy angle increases with the increase of tube row number, which is consistent with the field synergy principle. In all the studies presented below, the change trend of the average synergy angle of every cases can be well described by the field synergy principle. So, the average synergy angle will not be presented and mentioned again for simplicity of presentation.

4.2.2. The effect of longitudinal tube pitch

The non-dimensional longitudinal tube pitch varied from 1.90 to 2.13. As shown in Fig. 11 both j factor and f factor decrease with the increase of the longitudinal tube pitch. j factor decreases about 10 percent and f factor decreases about 9 percent. This can be explained that heat transfer and pressure drop are both higher in the region around the tube. As a result, adding plate fin far from the tube will worsen heat transfer and decrease friction factor.

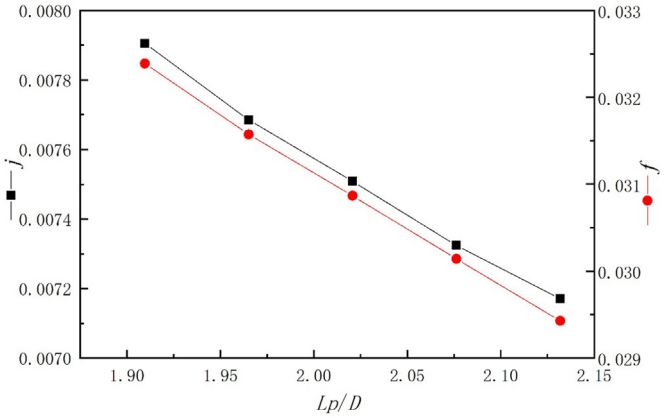

Fig. 11. The effect of longitudinal tube pitch on *j* factor and *f* factor.

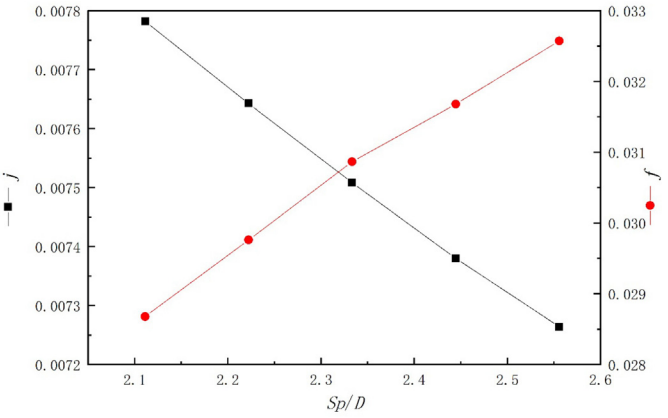

Fig. 12. The effect of spanwise tube pitch on *j* factor and *f* factor.

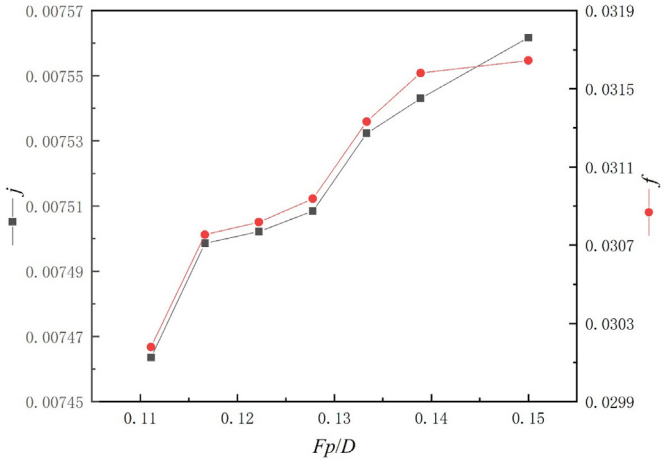

Fig. 13. The effect of fin pitch on *j* factor and *f* factor.

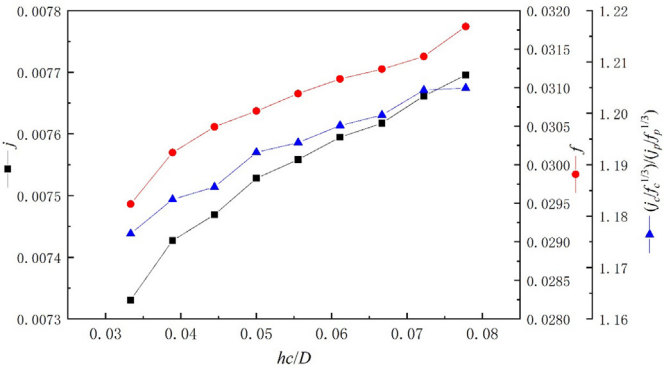

Fig. 14. The effect of height of strips on *j* factor, *f* factor and PEF.

4.2.3. The effect of spanwise tube pitch

The spanwise tube pitch changed from 38 mm to 46 mm to study its effects. From Fig. 12 we can see that the changing trends of *j* factor and *f* factor are totally different. With spanwise tube pitch increasing from 38 mm to 46 mm, *j* factor decreases by 7% and *f* factor increases by 13%. With the increase in spanwise pitch the percentage of the around-tube area decreases and that of the plain fin increases hence the averaged heat transfer coefficient decreases. On the other hand, at the same Reynolds number with the increase of the spanwise pitch the increase of ratio between minimum cross section flow area and heat transfer area outside the tube is more significant than the decrease of pressure drop due to larger cross section area which leads to an increase of friction factor (see Eq. (19)).

4.2.4. The effect of fin pitch

In the investigation of the fin pitch effect on heat transfer and fluid flow, the non-dimensional fin pitch varied from 0.111 to 0.139. Relationships of fin pitch to both *j* factor and *f* factor are shown in Fig. 13. Both the *j* factor and the *f* factor have a minor increase (about 1–2%) with the increase of the fin pitch in the studied range of fin pitch. The effect of fin pitch on heat transfer coefficient could almost be ignored. Study result in paper [31] also shows that when fin pitch is large enough the effect of fin pitch is not significant.

4.2.5. The effect of strip height

For investigating the effect of strip height on heat transfer and fluid flow, the non-dimensional slit height varied from 0.033 to 0.078. The result is shown in Fig. 14. Both the *j* and *f* factors increase with the increase of strip height. As mentioned above, the convex plate can enhance heat transfer from two aspects: firstly, disturbing the air flow passing over the strip; secondly, preventing the air from flowing away from the tube. With the increase of strip height, effects of both two aspects are enhanced. These reasons make the changing trend shown in the figure. As shown in Fig. 14, within the studied strip height range, the factor $(j_c/f_c^{1/3})/(j_p/f_p^{1/3})$ is always larger than 1 which means that the heat transfer under the same pumping power can always be enhanced compared with plain fin. Further more, the increasing trend of the factor with the increase of strip height shows that the heat transfer under the same pumping power can be further enhanced by increasing the strip height. The result that the factor is almost the same for the last two points may suggest that the enhance effect for overall performance reaching maximum when strip height between 1.3 mm and 1.4 mm.

4.2.6. The effect of frontal/rear strip length

The length of strip (S_1 and S_2) (see Fig. 2(b)) varied from 0 mm to 14 mm to investigate its effect on the *j* and *f* factors. The results are shown in Figs. 15 and 16, where the way of changing S_1 and S_2 are shown. It can be seen that both *j* factor and *f* factor increase with the increase of S_1 and S_2. As mentioned in Section 4.2.5, heat transfer can be enhanced by two aspects. The strip can roughly be separated into two parts: Part I nearly perpendicular to the air flow direction and Part II nearly parallel to air flow direction. Part I mainly disturbs the air flowing over the strip and enhances heat transfer after the strip. Part II mainly guides the air flow and increases the air flowing around the tube. For the rear slit, Part I can guide the air flowing into the wake region behind the tube which has significant effect to enhance heat transfer. Therefore the length

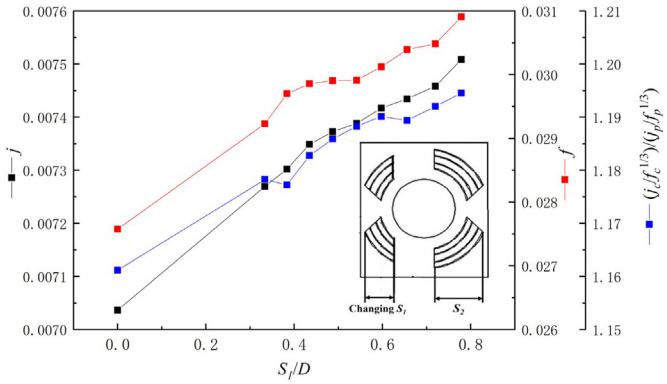

Fig. 15. The effect of length of frontal strips on j factor, f factor and PEF.

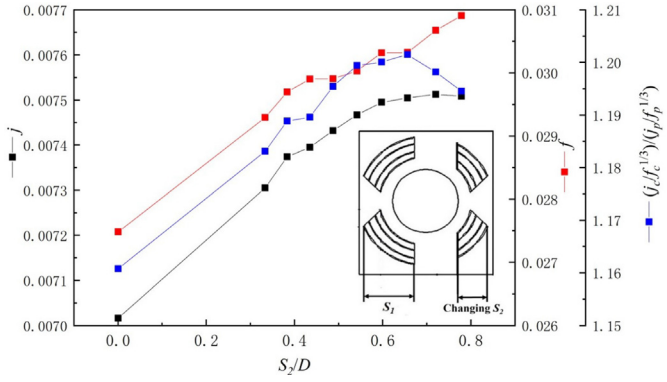

Fig. 16. The effect of length of rear strips on j factor, f factor and PEF.

of both front and rear slits has positive effect on enhancing heat transfer. From the view of overall performance, the heat transfer under the same pumping power increases almost linearly with the increase of frontal strip and the best heat transfer performance under the same pumping power can be get when S_2/D between 0.6 and 0.7.

4.3. Multiple correlation

Based on the previous study, final correlations are given by multiple regression method. It should be noted that the length of the frontal and rear strip starts from zero. To correlate the effect of S_1/D and S_2/D, following scheme is adopted.

$$j - j_{S=0} = c + a\left(\frac{S}{D}\right)^{b} \tag{24}$$

The final correlations are proposed as follows:

For $S_2/D = 0$ to 0.5973

$$j = 0.043Re^{-0.58}N^{-0.18}\left(\frac{L_p}{D}\right)^{-0.88}\left(\frac{S_p}{D}\right)^{-0.36} \times\left[12.3+\left(\frac{S_1}{D}\right)^{0.75}\right]\left[9.4+\left(\frac{S_2}{D}\right)^{0.82}\right] \tag{25}$$

For S_2/D>0.5973 to 0.7785

$$j = 0.029Re^{-0.58}N^{-0.18}\left(\frac{L_p}{D}\right)^{-0.88}\left(\frac{S_p}{D}\right)^{-0.36} \times\left[12.3+\left(\frac{S_1}{D}\right)^{0.75}\right]\left[13.7+\left(\frac{S_2}{D}\right)^{0.12}\right] \tag{26}$$

For $S_2/D = 0$ to 0.7785

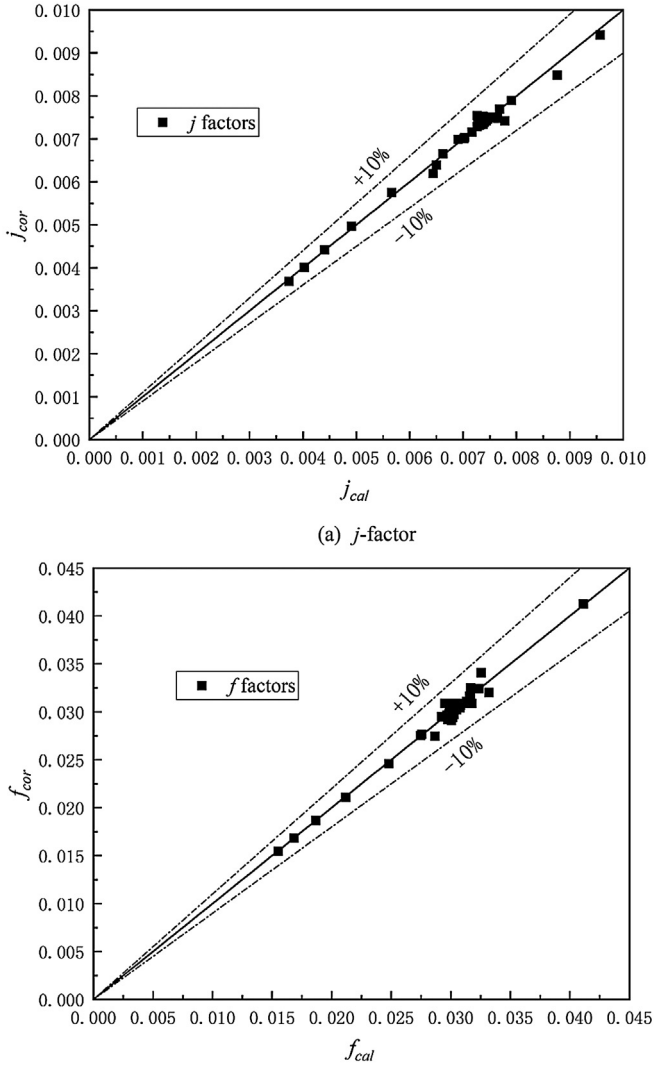

Fig. 17. Comparison between predicted results and numerical results.

$$f = 0.225Re^{-0.61}N^{-0.05}\left(\frac{F_p}{D}\right)^{0.16}\left(\frac{L_p}{D}\right)^{-0.87}\left(\frac{S_p}{D}\right)^{0.67} \times\left[7.4+\left(\frac{S_1}{D}\right)^{0.68}\right]\left[7.0+\left(\frac{S_2}{D}\right)^{0.65}\right] \tag{27}$$

The application range of the correlations is listed as follows: Re=6000 to 34000, N = 2 to 12, D = 18 mm, F_p/D = 0.111 to 0.139, H_c/D = 0.033 to 0.072, S_1/D = 0 to 0.7785, L_p/D = 1.91 to 2.13, S_p/D = 2.11 to 2.44. If the number of rows is larger than 12, the j and f factors can be calculated by setting N equal to 12.

The comparisons between predicted results and numerically calculated results are shown in Fig. 17. All deviations are within 10% and actually the maximum deviations for j factor and f factor are 4.6% and 4.7%, respectively.

5. Conclusion

Three dimensional numerical investigations were made by software FLUENT for turbulent heat transfer and pressure drop of a new strip fin in which there are four convex strips around each tube. The realizable k-ε turbulence model is adopted. Some conclusions can be made as follows:

1 The heat transfer and pressure drop of this new strip fin are 25% and 33% higher than those of plain fin, respectively.
2 The air flows over the new strip fin and the heat transfer between them come into full development stage after 12 rows.
3 The effects of six geometric parameters (F_p, H_c, L_p, S_p, S_1, S_2) on the heat transfer and friction factor are investigated. It is found that for j factor S_1, S_2, F_p and H_c have strong positive effects, while L_p and S_p have negative effects; The friction factor increases with the increase of S_p, S_1, S_2, F_p and H_c, while decrease with the increase of L_p. Among the six parameters, the effects of F_p and H_c are quite weak for both j and f.
4 This new strip fin can enhance heat transfer under both identical pressure drop and identical pumping power conditions compared with plain fin. Higher Reynolds number can obtain better heat transfer performance under these two constraint conditions. The recommended strip height and length of rear strip are 1.3 mm and 12 mm respectively. Increasing the length of frontal strip can always increase the heat transfer under the same pumping power within the studied range in this paper.
5 In the developing and fully developed air flow and heat transfer regions, the j and f factors can be well correlated by Eqn 25, 26 and 27, respectively.

Declaration of Competing Interest

None.

Acknowledgement

This work was supported by the Key Research and Development Program of Shaanxi Province (2019TSLGY05-07),the Foundation for Innovative Research Groups of the National Natural Science Foundation of China (No. 51721004) and 111 Project (B16038).

References

[1] W.Q. Tao, W.W. Jin, Y.L. He, Z.G. Qu, C.C. Zhang, Optimum design of two-row slotted fin surface with X-shape strip arrangement positioned by "front coarse and rear dense" principle, part I: physical/mathematical models and numerical methods, Numerical Heat Transfer, Part A 50 (2006) 731–749.
[2] J.P. Joule, On the surface-condensation of steam, in: Philos. Trans. R. Soc., 151, London, 1861, pp. 133–160.
[3] W.Nakayama, L.P.Xu, Enhanced fins for air-cooled heat exchangers-heat transfer and friction correlations, 1st ASME/JSME Thermal Engineering Joint Conference 1(1983) 495–502.
[4] J.Y.Yun, K.S.Lee, Investigation of heat transfer characteristics on various kinds of fin-and-tube heat exchangers with interrupted surfaces, Int. J. Heat Mass Transf.42 (199) 2375–2385.
[5] C.C. Wang, C.J. Lee, C.T. Chang, S.P. Lin, Heat transfer and friction correlation for compact louvered fin-and-tube heat exchangers, Int. J. Heat Mass Transf.42 (1999) 1945–1956.
[6] C.C. Wang, W.H. Tao, C.J. Chang, An investigation of the airside performance of the slit fin-and-tube heat exchangers, Int. J. Ref. 22 (1999) 595–603.
[7] Y.J. Du, C.C. Wang, An experimental study of the airside performance of the superslit fin-and-tube heat exchangers, Int. J. Heat Mass Transf.43 (2000) 4475–4482.
[8] K. Balatka, S. Mochizuki, A. Murata, Investigation of flow behavior and heat transfer in tube and slit-fin heat exchangers, J. Flow Visual. Image Process.7 (2000) 89–101.
[9] T. Matsuda, A. Ishibashi, S. Lee, H. Shiba, Heat transfer and pressure drop characteristics of cross stair slit fin, Int. Ref. Air Condition. Conf. Purdue July (2010) 12–15.
[10] N.H. Kim, T. Kim, An experimental investigation on the airside performance of fin-and-tube heat exchangers having slit fins under wet condition, J. Mech. Sci. Tech.29 (11) (2015) 5011–5019.
[11] N.H. Kim, An experimental investigation on the airside performance of fin-and-tube heat exchangers having radial slit fins under wet condition, J. Therm. Sci. Tech.11 (2016) 1–17.
[12] X.K. Ma, G.L. Ding, Y.M. Zhang, K.J. Wang, Airside heat transfer and friction characteristics for enhanced fin-and-tube heat exchanger with hydrophilic coating under wet conditions, Int. J. Refrig.30 (2007) 1153–1167.
[13] Z.G. Qu, W.Q. Tao, Y.L. He, Simulation on laminar heat transfer and fluid flow characteristics of strip fin surface with X-arrangement of strips, ASME J. Heat Transf.126 (2004) 697–707.
[14] Z.Y. Guo, D.Y. Li, B.X. Wang, A novel concept for convective heat transfer enhancement, Int. J. Heat Mass Transf. 41 (14) (1998) 2221–2225.
[15] Z.Y. Guo, W.Q. Tao, R.K. Shah, The field synergy (coordination) principle and its applications in enhancing single phase convective heat transfer, Int. J. Heat Mass Transf. 48 (9) (2005) 1797–1807.
[16] Y.P. Cheng, Z.G. Qu, W.Q. Tao, Y.L. He, Numerical design of efficient slotted fin surface based on the field synergy principle, Numer. Heat Transf. Part A 45 (6) (2004) 517–538.
[17] J.J. Zhou, W.Q. Tao, Three dimensional numerical simulation and analysis of the airside performance of slotted fin surfaces with radial strips, Eng. Comput.22 (2005) 940–957.
[18] W.W. Jin, Y.L. He, Z.G. Qu, C.C. Zhang, W.Q. Tao, Optimum design of two-row slotted fin surface with X-shape strip arrangement positioned by "front coarse and rear dense" principle, Part II:Results and discussion, Numerical Heat Transfer, Part A 50 (2006) 751–771.
[19] W.Q. Tao, Y.P. Cheng, T.S. Lee, The influence of strip location on the pressure drop and heat transfer performance of a slotted fin, Numer. Heat Transf.Part A 52 (2007) 463–480.
[20] J.M. Wu, W.Q. Tao, Numerical study on laminar convection heat transfer in a rectangular channel with longitudinal vortex generator, Part A: verification of field synergy principle, Int. J. Heat Mass Transf.51 (2008) 1179–1191.
[21] J.M. Wu, W.Q. Tao, Numerical study on laminar convection heat transfer in a rectangular channel with longitudinal vortex generator, Part A: parametric study of major influence factors, Int. J. Heat Mass Transf.51 (2008) 3683–3692.
[22] J. Li, S.F. Wang, J.F. Chen, Y.G. Lei, Numerical study on a slit fin-and-tube heat exchanger with longitudinal vortex generators, Int. J. Heat Mass Transf.54 (2011) 1743–1751.
[23] J.F. Fan, L.He Y, W.Q. Tao, Application of combined enhanced techniques for design of highly efficient air heat transfer surface, Heat Transf. Eng.33 (1) (2012) 52–62.
[24] X.H. Wu, W.H. Zhang, Y.L. Lu, Q.P. Gou, Z.M. Luo, Performance evaluation and optimization of semi-dimpled slit fin, Heat Mass Transf.50 (2014) 1251–1259.
[25] X.H. Wu, W.H. Zhang, Q.P. Gou, Z.M. Luo, Y.L. Lu, Numerical simulation of heat transfer and fluid flow characteristics of composite fin, Int. J. Heat Mass Transf.75 (2014) 414–424.
[26] M.J. Li, W.J. Zhou, J.F. Zhang, J.F. Fan, Y.L. He, W.Q. Tao, Heat transfer and pressure performance of a plain fin with radiantly arranged winglets around each tube in fin-and-tube heat transfer surface, Int. J. Heat Mass Transf.70 (2014) 734–744.
[27] S. Sarpotdar, D. Nasuta, V. Aute, CFD based comparison of slit fin and louver fin performance for small diameter (3 mm to 5 mm) heat exchangers, 16th Int. Ref. Air Condition. Conf. Purdue July (11–14) (2016) 2361–2362.
[28] D.H. Park, D.B. Lee, E.R. Seo, Y.J. Park, Study on the heat transfer and fluid flow characteristics in V-shaped corrugated composite fin, Appl. Therm. Eng. 102 (2016) 293–301.
[29] M. Mutlu, M. Kilic, Three-dimensional conjugate numerical analysis of fin and tube heat exchangers with various fin thermal conductivity values and geometric parameters, J. Therm. Sci. Tech.36 (1) (2016) 85–98.
[30] M. Zeng, W.Q. Tao, Numerical verification of the field synergy principle for turbulent flow, J, Enhanc. Heat Transf.11 (4) (2004) 451–457.
[31] Y.L. He, W.Q. Tao, F.Q. Song, W. Zhang, Three-dimensional numerical study of heat transfer characteristics of plain plate fin-and-tube heat exchangers from view point of field synergy principle, Int. J. Heat Fluid Flow 26 (2005) 459–473.
[32] C. Allison, B. Dally, Effect of a delta-winglet vortex pair on the performance of a tube-fin heat exchanger, Int. J. Heat Mass Transf.50 (25–26) (2007) 5065–5072.
[33] Z.X. Li, Z.Y. Guo, Field Synergy Principle for Optimization of Convective Heat Transfer, Science Press, Beijing, 2010 Section 2.3 (in Chinese).
[34] X. Li, Y.L. He, W.Q. Tao, Analysis and extension of field synergy principle (FSP) for compressible boundary-layer heat transfer, Int. J. Heat Mass Transf.84 (2015) 1061–1069.
[35] Y.L. He, W.Q. Tao, Convective heat transfer enhancement: mechanism, techniques and performance evaluation, Adv. Heat Transf.46 (2014) 87–186.
[36] W.Q. Tao, Numerical Heat Transfer, Xi'an Jiaotong University Press, Xi'an, 2001 2nd edition.
[37] T.H. Shih, W.W. Liou, A. Shabbir, Z. Yang, J. Zhu, A new k-ε eddy viscosity model for high Reynolds number turbulent flows—Model development and validation, Comput. Fluids 24 (3) (1995) 227–238.
[38] Xiao-Yu Li, Zhao-Hui Li, Wen-Quan Tao, Experimental study on heat transfer and pressure drop characteristics of fin-and-tube surface with four convex-strips around each tube, Int. J. Heat Mass Transf.116 (2018) 1085–1095.